Journal of the Optical Society of America B

OPTICAL PHYSICS

What optical fiber modes reveal: group velocity and effective index for external perturbations

SWAATHI UPENDAR,[1] MARKUS A. SCHMIDT,[2,3] AND THOMAS WEISS[1,*]

[1] 4th Physics Institute and Research Center SCoPE, University of Stuttgart, Pfaffenwaldring 57, 70569 Stuttgart, Germany
[2] Leibniz Institute of Photonic Technology, e.V. Albert-Einstein-Str. 9, 07745 Jena, Germany
[3] Otto Schott Institute of Material Research, Friedrich Schiller University, Fraunhoferstr. 6, 07743 Jena, Germany
*Corresponding author: t.weiss@pi4.uni-stuttgart.de

Received 21 December 2020; revised 4 February 2021; accepted 15 February 2021; posted 16 February 2021 (Doc. ID 418272); published 8 March 2021

Precise control of fiber modes and their dispersion is essential, particularly for fields such as nonlinear frequency conversion or biosensing, both of which often require extensive and time-consuming simulations for design optimization. Here, we develop a first-order perturbation theory for predicting the effective index of bound and leaky fiber modes that is applicable for arbitrary global perturbations as long as the perturbations in the external surrounding are constantly homogeneous and isotropic deviations from the unperturbed fiber. This includes changes not only in permittivity and permeability, but also in wavelength. Thus, we are able to calculate the group velocity solely from the field distributions of the fiber modes at a single wavelength, which therefore allows for large-scale parameter sweeps for accurately managing dispersion. We demonstrate the capabilities of our theory for various trial systems such as step index fibers, photonic crystal fibers, and light cages.

https://doi.org/10.1364/JOSAB.418272

1. INTRODUCTION

Optical fibers represent one of the most successful photonic devices and guide light in a central core surrounded by a cladding. Particularly with respect to modal engineering, this cladding could be a homogeneous material, as in the case of step index and capillary fibers [1], or comprise complex structures, such as the periodic arrangements of holes or strands in microstructured fibers [2]. The guiding properties of both kinds of fibers are impacted by the constituent materials that comprise the core and cladding and react to changes of these materials. Due to the strong susceptibility of the core mode to changes of the refractive index, optical fibers represent one promising platform for bioanalytical or medical applications [3–6]. Furthermore, the dispersion properties of the fiber modes can be accurately tuned over a wide range in complex fiber geometries, which is essential, particularly in the context of ultrafast nonlinear optical effects such as supercontinuum generation [7] or four-wave mixing [8].

All of the mentioned applications demand optimizing the fiber structures via extensive numerical simulations, which can be time-consuming and may not be used for large-scale parameter sweeps. Here, the perturbation theory is known to be a suitable approach for such tasks, since it can significantly reduce the simulation time and complexity [9], thus providing a pathway toward design optimization. Optical perturbation theories based on the resonant states, also known as quasi-normal modes, are broadly used for optical resonators [10–12]. However, care has to be taken with respect to the normalization of unbound modes. These modes are leaky in the sense that they radiate part of their energy to the far field. Hence, their field distributions grow with distance to the resonator. In recent years, different approaches have been developed in order to normalize these modes correctly [13–16], resulting in accurate predictions for various refractive index sensors [9,17–19]. We have adapted the analytical normalization of Ref. [16] to fiber and leaky waveguide geometries [20], which allows for predicting changes of the effective index of bound and leaky fiber modes in the case of modifications of the refractive index with perturbation theory, as well as for describing the nonlinear pulse propagation of leaky modes [21]. Common to all of these perturbative approaches is that they deal exclusively with perturbations in the interior of the structure. This limitation is overcome for optical resonators in Ref. [22], where the resonance frequency shifts, and linewidth changes are predicted correctly for homogeneous and isotropic perturbations in the exterior.

More specifically, the infinite volume integral over perturbations in the exterior is replaced in Ref. [22] by an integral over the boundary of a finite volume. We adapt this approach to propagating modes in fiber geometries. An interesting fact is that for these modes, the wavelength is an input parameter to Maxwell's equations similar to the refractive index, which, in turn, means that changes in wavelength can be treated as a perturbation. This allows for an exact prediction of the group velocity based on calculating the fiber modes and their field

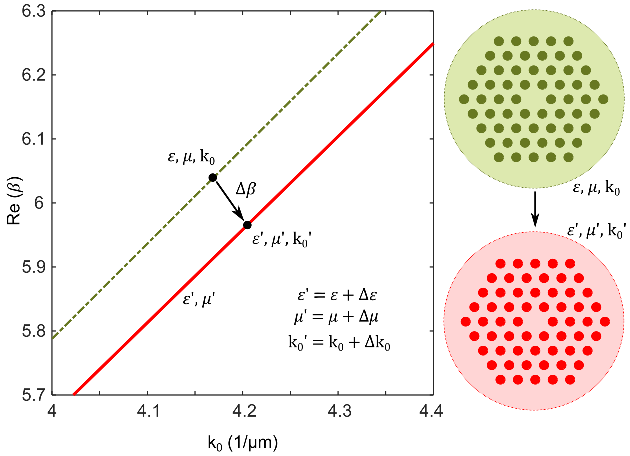

Fig. 1. Real part of the propagation constant β as a function of wavenumber k_0 for an unperturbed photonic crystal fiber (see schematic on the right) with permittivity ε and permeability μ (green dashed–dotted line) and for a perturbed fiber with permittivity ε' and permeability μ' (red solid line). Via our first-order perturbation theory, we can predict the change of the propagation constant $\Delta\beta$ not only for small modifications $\Delta\varepsilon$ and $\Delta\mu$ of the permittivity and permeability, respectively, but also for wavenumber changes Δk_0. The radius of the inclusions in the photonic crystal fiber is 0.5 µm, and the pitch is 2.3 µm. The unperturbed fiber in the dispersion plot has a background refractive index of 1.47, while the perturbed fiber has a background refractive index of 1.44. The index of the inclusions (holes) is one.

distributions at a single frequency, without having to repeatedly solve Maxwell's equations for different wavelengths and approximating derivatives with respect to wavelengths by finite differences. Hence, we can predict the propagation constant for small changes in the wavelength, permittivity, and permeability (see Fig. 1), as long as the modification of Maxwell's equations is homogeneous and isotropic in the exterior.

2. THEORY

In fiber geometries, the permittivity and permeability tensors, ε and μ, respectively, are translationally symmetric along one spatial direction, which we choose to be the z direction. Hence, we can apply the Fourier transformation

$$\hat{f}(\mathbf{r}_{\|};\beta)=\frac{1}{2\pi}\int_{-\infty}^{\infty}\mathrm{d}z f(\mathbf{r}_{\|};z)e^{-i\beta z}, \tag{1}$$

with $\mathbf{r}_{||}$ being the projection of $\mathbf{r}$ to the xy plane, and the hat denoting Fourier transformed quantities. Thus, Maxwell's equations can be written in the frequency domain [time dependence $\exp(-i\omega t)$, Gaussian units] as

$$\hat{\mathbb{M}}_0(\mathbf{r}_{||};\beta)\hat{\mathbb{F}}=\hat{\mathbb{J}}(\mathbf{r}_{||}), \tag{2}$$

where

$$\hat{\mathbb{M}}_0(\mathbf{r}_{||};\beta)=\begin{pmatrix} k_0\varepsilon & -\hat{\nabla}_\beta\times \\ -\hat{\nabla}_\beta\times & k_0\mu \end{pmatrix},\quad \text{with } \hat{\nabla}_\beta=\begin{pmatrix}\partial_x\\ \partial_y \\ i\beta\end{pmatrix}, \tag{3}$$

and

$$\hat{\mathbb{F}}=\begin{pmatrix}\hat{\mathbb{E}}\\ i\hat{\mathbb{H}}\end{pmatrix}\quad\text{and}\quad \hat{\mathbb{J}}(\mathbf{r}_{||})=\begin{pmatrix}\hat{\mathbb{J}}\\ 0\end{pmatrix}. \tag{4}$$

Here, $\hat{\mathbb{E}}$ is the electric field, $\hat{\mathbb{H}}$ is the magnetic field, $k_0=\omega/c$ is the wavenumber, while $\varepsilon=\varepsilon(\mathbf{r}_{||})$ and $\mu=\mu(\mathbf{r}_{||})$ denote the permittivity and permeability tensors, respectively. Furthermore, $\hat{\mathbb{J}}=-4\pi i\hat{\mathbf{j}}/c$ is the source of the fields, where $\hat{\mathbf{j}}$ is the electric current. Resonant states are solutions of Maxwell's equations in the absence of source terms that satisfy outgoing boundary conditions in the transversal directions with complex propagation constants β_m:

$$\hat{\mathbb{M}}_0(\mathbf{r}_{||};\beta_m)\hat{\mathbb{F}}_m=0. \tag{5}$$

We now introduce a perturbation in our system as a change in permittivity ($\varepsilon\to\varepsilon+\Delta\varepsilon$) or permeability ($\mu\to\mu+\Delta\mu$) or a change in wavenumber ($k_0\to k_0+\Delta k_0$) that can be converted to a change in wavelength. We also introduce a factor Λ to turn the perturbation on and off. The new perturbed operator $\hat{\mathbb{M}}$ can be written as

$$\hat{\mathbb{M}}=\hat{\mathbb{M}}_0+\Lambda\Delta\hat{\mathbb{M}}, \tag{6}$$

where

$$\Delta\hat{\mathbb{M}}\equiv\Delta\hat{\mathbb{M}}_{k_0}+\Delta\hat{\mathbb{M}}_{\varepsilon}+\Delta\hat{\mathbb{M}}_{\mu}, \tag{7}$$

with

$$\Delta\hat{\mathbb{M}}_{k_0}=\begin{pmatrix}\Delta k_0\varepsilon & 0\\ 0 & \Delta k_0\mu\end{pmatrix},\quad \Delta\hat{\mathbb{M}}_{\varepsilon}=\begin{pmatrix}k_0\Delta\varepsilon & 0\\ 0 & 0\end{pmatrix},\quad \Delta\hat{\mathbb{M}}_{\mu}=\begin{pmatrix}0 & 0\\ 0 & k_0\Delta\mu\end{pmatrix}. \tag{8}$$

Henceforth, we consider the subscript ν for the resonant states of the perturbed system, which satisfy

$$\hat{\mathbb{M}}(\mathbf{r}_{||};\beta_\nu)\hat{\mathbb{F}}_\nu=0. \tag{9}$$

For every solution $\hat{\mathbb{F}}_m$ of Eq. (5) with propagation constant β_m, there exists a reciprocal conjugate solution $\hat{\mathbb{F}}_m^{\mathrm{R}}$ with propagation constant $-\beta_m$. We now use the forward and reciprocal conjugate, i.e., backward propagating modes as in Ref. [20], to get

$$\hat{\mathbb{F}}_\nu\cdot\hat{\mathbb{M}}_0(\mathbf{r}_{||};\beta_m)\hat{\mathbb{F}}_m^{\mathrm{R}}-\hat{\mathbb{F}}_m^{\mathrm{R}}\cdot\hat{\mathbb{M}}(\mathbf{r}_{||};\beta_\nu)\hat{\mathbb{F}}_\nu=0. \tag{10}$$

Integrating over a circular surface S of radius R in the xy plane that encloses all regions of spatial inhomogeneities and applying vector identities, we obtain

$$\begin{aligned}&R\int\mathrm{d}\phi(\hat{E}_{\nu\phi}\hat{H}^{\mathrm{R}}_{mz}-\hat{E}_{\nu z}\hat{H}^{\mathrm{R}}_{m\phi}-\hat{E}^{\mathrm{R}}_{m\phi}\hat{H}_{\nu z}+\hat{E}^{\mathrm{R}}_{mz}\hat{H}_{\nu\phi})_{\rho=R}\\ &+i(\beta_\nu-\beta_m)\int_S\mathrm{d}A(\hat{E}_{\nu\rho}\hat{H}^{\mathrm{R}}_{m\phi}-\hat{E}_{\nu\phi}\hat{H}^{\mathrm{R}}_{m\rho}-\hat{E}^{\mathrm{R}}_{m\rho}\hat{H}_{\nu\phi}+\hat{E}^{\mathrm{R}}_{m\phi}\hat{H}^{+}_{\nu\rho})\\ &+i\Lambda\int\mathrm{d}A\quad\hat{\mathbb{F}}^{\mathrm{R}}_m\cdot\Delta\hat{\mathbb{M}}\hat{\mathbb{F}}_\nu=0,\end{aligned} \tag{11}$$

where we have introduced cylindrical coordinates ρ and ϕ for the sake of convenience.

Similar to perturbation theories in quantum mechanics [23] and the first-order external perturbation theory in Ref. [22], we write the propagation constant β and fields of the perturbed system as a power series, i.e.,

$$\beta_v = \beta_m + \Lambda\beta_m^{(1)} + O(\Lambda^2) + \cdots , \tag{12}$$

and

$$\hat{\mathbb{F}}_v = \hat{\mathbb{F}}_m + \Lambda\hat{\mathbb{F}}_m^{(1)} + O(\Lambda^2) + \cdots . \tag{13}$$

Substituting these expansions in Eq. (11) and equating the zero-order terms with respect to Λ, we obtain

$$R\int \mathrm{d}\phi(E_\phi H_z^{\mathrm{R}} - E_z H_\phi^{\mathrm{R}} - E_\phi^{\mathrm{R}} H_z + E_z^{\mathrm{R}} H_\phi)_{\rho=R} = 0. \tag{14}$$

For the sake of convenience, we exclude the hat and subscript m. Using the symmetries of the system [20], the reciprocal conjugate (backward propagating) modes can be converted to forward propagating modes by multiplying a factor of -1 to the in-plane components of the magnetic field and the z component of the electric field. The other components remain unchanged. Hence, Eq. (14) is trivially fulfilled. We now equate the first-order terms for Λ to get

$$\begin{aligned} &R\int \mathrm{d}\phi\{E_\phi H_z^{(1)} + E_z H_\phi^{(1)} - E_\phi^{(1)} H_z - E_z^{(1)} H_\phi\}_{\rho=R} \\ &+ 2i\beta_m^{(1)}\int_S \mathrm{d}A(E_\rho H_\phi - E_\phi H_\rho) - i\int_S \mathrm{d}A\mathbb{F}_m^{\mathrm{R}}\cdot\Delta\mathbb{MF}_m = 0. \end{aligned} \tag{15}$$

We evaluate the first-order correction terms in Eq. (15) in order to obtain the first-order correction term of the propagation constant. The details of deriving the first-order correction terms for the fields are described in Appendix A.

The first-order correction term then yields

$$\beta_m^{(1)} = \frac{\int \mathrm{d}A\mathbb{F}_m^{\mathrm{R}}\cdot\Delta\mathbb{MF}_m + \frac{\Delta\varepsilon}{\varepsilon}L_1^\varepsilon + \frac{\Delta\mu}{\mu}L_1^\mu + \frac{\Delta k_0}{k_0}L_1^{k_0}}{S_0 + L_0}, \tag{16}$$

where $\Delta\varepsilon$ and $\Delta\mu$ are homogeneous and isotropic modifications of the permittivity and permeability in the surroundings, respectively. Furthermore, L_1^ε, L_1^μ, and $L_1^{k_0}$ are defined as

$$L_1^\varepsilon = \beta I_0 + I_1 - I_E, \tag{17}$$

$$L_1^\mu = \beta I_0 + I_1 - I_H, \tag{18}$$

$$L_1^{k_0} = L_1^\varepsilon + L_1^\mu, \tag{19}$$

with I_0, I_1, I_E, and I_H as line integrals in the exterior:

$$I_0 = \frac{i\varepsilon\mu k_0^2}{\varkappa^4}\int \mathrm{d}\phi\left(E_z\frac{\partial H_z}{\partial\phi} - H_z\frac{\partial E_z}{\partial\phi}\right)_{\rho=R}, \tag{20}$$

$$\begin{aligned} I_1 = \frac{ik_0^3R^2\varepsilon\mu}{2\varkappa^4}\int \mathrm{d}\phi\varepsilon\Bigg\{&\left[\left(\frac{\partial E_z}{\partial\rho}\right)^2 - \rho E_z\frac{\partial}{\partial\rho}\left(\frac{1}{\rho}\frac{\partial E_z}{\partial\rho}\right)\right] \\ &+ \mu\left[\left(\frac{\partial H_z}{\partial\rho}\right)^2 - \rho H_z\frac{\partial}{\partial\rho}\left(\frac{1}{\rho}\frac{\partial H_z}{\partial\rho}\right)\right]\Bigg\}_{\rho=R}, \end{aligned} \tag{21}$$

$$I_E = \frac{iRk_0\varepsilon}{\varkappa^2}\int \mathrm{d}\phi\left(E_z\frac{\partial E_z}{\partial\rho}\right)_{\rho=R}, \tag{22}$$

$$I_H = \frac{iRk_0\mu}{\varkappa^2}\int \mathrm{d}\phi\left(H_z\frac{\partial H_z}{\partial\rho}\right)_{\rho=R}. \tag{23}$$

Here, $\varkappa$ is defined as $\varkappa^2 = \varepsilon\mu k_0^2 - \beta^2$, with ε and μ being the permittivity and permeability in the surroundings. The radius R defines the circular area over which the surface and line integrals are calculated. The circle can be arbitrarily large, except for the condition that it must comprise all regions of spatial inhomogeneities. The terms in the denominator of Eq. (16) are defined as

$$S_0 = 2i\int_S \mathrm{d}A(E_\rho H_\phi - E_\phi H_\rho), \tag{24}$$

and

$$L_0 = \left(1 + \frac{\beta^2}{\varepsilon\mu k_0^2}\right)I_0 + \frac{2\beta}{k_0^2\varepsilon\mu}I_1. \tag{25}$$

Interestingly, it turns out that the denominator of Eq. (16) is the expression for the normalization of leaky modes, as derived in Ref. [20]. This normalization automatically reappears as part of the first-order perturbation theory.

3. PERTURBATION IN PERMITTIVITY

Let us consider only an ε perturbation in our system. Thus, the $\Delta\mu$ and Δk_0 terms go to zero, and we are left with a surface and line integral for only the ε perturbation in Eq. (16). The surface term for a purely ε perturbation is given by

$$S_1^\varepsilon = ik_0\int_S \mathrm{d}A\mathbb{E}_m^R\cdot\Delta\varepsilon\mathbb{E}_m. \tag{26}$$

We see that the surface integral term for external perturbation is identical to the previously derived surface term for internal perturbations in Ref. [20], with an additional line integral term enclosing the surface of integration. Both the surface and line terms are calculated at an arbitrary radius R taken outside the region of spatial inhomogeneities. Since the modes of fibers such as photonic crystal and capillary fibers are leaky in nature, the fields of these modes grow as we move radially away from the fiber core. Hence, both the surface and line integral terms are not independent of the radius of integration, as can be seen in Fig. 2 for an ε perturbation of unity in the entire system, for a higher-order leaky mode of a silica–air photonic crystal fiber with effective index $1.431 + 0.000342i$. We can see that both the surface (blue solid line) and line (red dashed line) integrals are growing as a function of the radius of integration, but their sum cancels out the increasing amplitude of the two integrals,

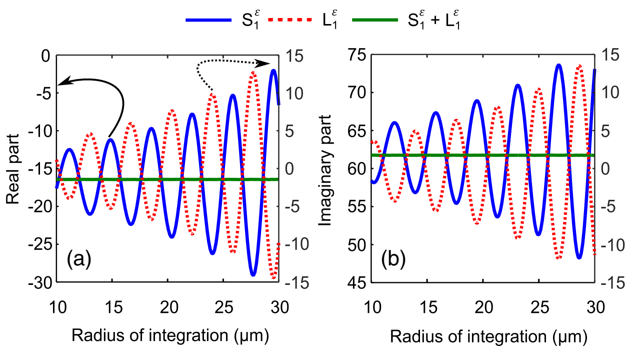

Fig. 2. (a) Real and (b) imaginary parts of the surface and line integral defined in Eqs. (26) and (17) for $\Delta\varepsilon = 1$ throughout the fiber as a function of the radius of integration for a higher-order leaky mode of a silica–air photonic crystal fiber. The fiber has four cladding rings with one missing inclusion as the core (see schematic in Fig. 1). The strand radius is 0.25 μm, and the pitch is 2.3 μm. The wavelength is 1 μm. It is evident that the surface and line integrals are growing with the radius of integration, but their sum cancels out this growth and results in a constant value.

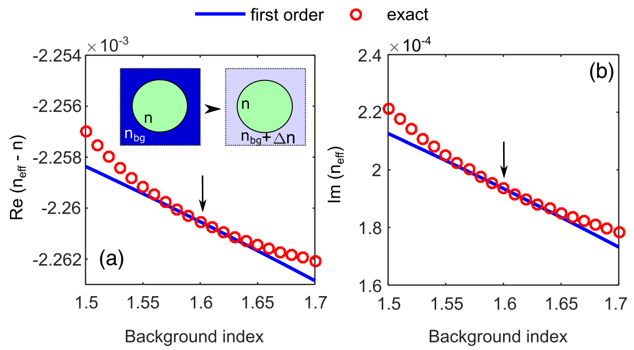

Fig. 3. Comparison of the (a) real and (b) imaginary parts of the effective index between the exact solution (red circles) and first-order perturbation (blue lines) as a function of the background refractive index of the fundamental core mode for a leaky step index fiber having $n < n_{\mathrm{bg}}$. Note that the y-axis scale in (a) is the difference of the effective and core indices n to make very small changes of the effective index visible when changing the background index n_{bg}. The radius of the core is 5 μm, and the wavelength is 1 μm. The unperturbed refractive indices are $n = 1.29$ (teflon AF) in the core and $n_{\mathrm{bg}} = 1.60$ (high index liquids [27]) in the surroundings, where the latter is indicated by the arrow.

yielding a constant value (green solid line) irrespective of the radius of integration. Note that the same radius of integration is applied to all quantities in Eq. (16), including its denominator.

We now apply the first-order perturbation theory for an external ε perturbation to a step index fiber. The chosen fiber has a teflon amorphous fluoropolymer (AF) core with an index of $n = 1.29$ [24] and a radius of $r = 5$ μm. We choose this fiber for its low index solid core that can be placed in high index liquids for refractive index sensing and other applications [25,26]. The unperturbed background index is $n_{\mathrm{bg}} = 1.60$. The schematic of this fiber can be seen in the inset of Fig. 3(a). In Figs. 3(a) and 3(b), we compare first-order perturbation theory (blue solid lines) and exact solutions (red circles) for the real and imaginary parts of the effective index, respectively, as a function of the background index for the fundamental core mode. The propagation constant is related to the effective index as $\beta = k_0 n_{\mathrm{eff}}$. We see that there is a good agreement between the exact solution and first-order perturbation theory for small index changes of the background material. The considered wavelength is 1 μm.

We now investigate a second example of a liquid surrounding a light-cage structure [28]. The schematic of the light cage is shown in the inset of Fig. 4(b). Since the light-cage structure is placed in the liquid, the background index is the same as the core index, which leads to higher field intensities interacting with the change in background index. The radius of the twelve strands of the light-cage structure is $r = 1$ μm, and the material of the strands is a polymer, as in Ref. [29]. We display the real and imaginary part of the effective index in Figs. 4(a) and 4(b), respectively, for exact numerical solutions and first-order perturbation theory. We can see that there is a very good agreement for the real part of the effective index in Fig. 4(a) due to its linear behavior as a function of the background index. Particularly, the slope of the numerical calculations is predicted correctly. The imaginary part also shows a good agreement as long as the perturbation is not too high. The unperturbed background index, indicated by the arrow in Fig. 4, is $n_{\mathrm{bg}} = 1.32$ (water [30]).

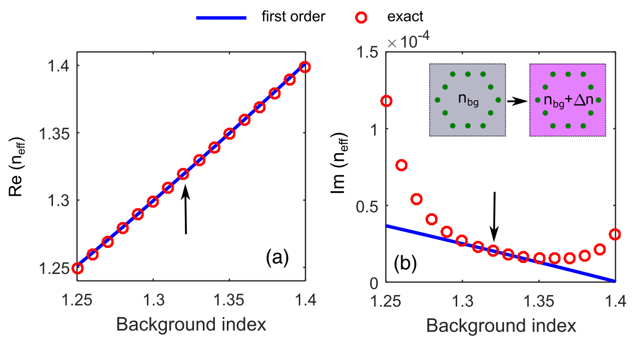

Fig. 4. Comparison of the (a) real and (b) imaginary parts of the effective index between the exact numerical solution (red circles) and first-order perturbation (blue lines) as a function of the background refractive index of the fundamental core mode for a light-cage structure embedded in a liquid medium. The strand radius is 1 μm, and the pitch (center-to-center) is 7 μm. The unperturbed background index is $n_{\mathrm{bg}} = 1.32$, indicated by the arrow in the plots. The wavelength is 1.50 μm.

4. WAVENUMBER PERTURBATION

Now let us consider only a k_0 perturbation, which essentially translates to a change in wavelength treated as a perturbation. We first investigate the case of a simple capillary fiber of radius $r = 5$ μm. The unperturbed wavelength is 1 μm. Figures 5(a) and 5(b) display the real and imaginary parts of the effective index, respectively, as a function of wavelength, for the exact solution and first-order perturbation. We see that there is a very good agreement between the two for both the real and imaginary parts, especially for small perturbations in wavelength. In fact, our perturbation theory can be used to calculate the exact value of the group velocity in fiber geometries as a single post processing step, in contrast to conventional numerical approaches.

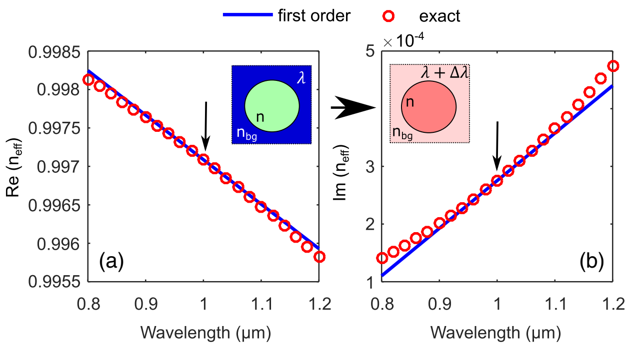

Fig. 5. Comparison of the (a) real and (b) imaginary parts of the effective index between the exact solution (red circles) and first-order perturbation (blue lines) as a function of wavelength for the fundamental core mode of a capillary fiber. The radius is 5 μm, and the unperturbed wavelength is 1 μm (indicated by the arrow). The refractive indices are $n = 1.00$ and $n_{bg} = 1.45$.

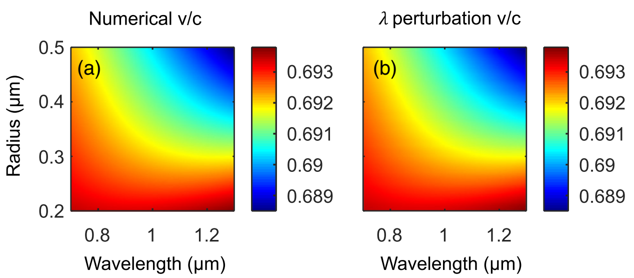

Fig. 6. Comparison of the group velocity v/c between the (a) numerical solution and (b) first-order perturbation as a function of wavelength and strand radius for the fundamental core mode of a silica–air photonic crystal fiber having four cladding rings and one missing inclusion as the core (see schematic of Fig. 1). The period is kept constant at 2.3 μm. The refractive index of silica is 1.44, while air has an index of one.

We now predict the values of the group velocity using the first-order perturbation and compare it with the numerical solutions for a silica–air photonic crystal fiber in Fig. 6. The background index is $n_{bg} = 1.44$ (silica), and the strands have $n = 1$ (air). The pitch is kept constant at 2.3 μm. We see in Figs. 6(a) and 6(b) that there is an excellent agreement of the group velocity for different strand radii and wavelengths. The group velocity is plotted in units of c, the speed of light. Hence, perturbation theory constitutes an efficient tool for predicting the group velocity of complicated fiber systems.

5. CONCLUSION

Precise knowledge of modal properties is essential for many photonic applications including bioanalytics, mode coupling, or ultrafast nonlinear frequency conversion. Here, we have derived a first-order perturbation theory for material perturbations of permittivity and permeability in the external surroundings. We have demonstrated good agreement between the propagation constants using exact solutions and first-order perturbation theory for small perturbations using different example fibers. We have also treated wavelength as a perturbation and shown that our theory is extremely valuable for calculating parameters such as group velocity as a simple post processing step. The results achieved will allow for speeding up simulations in order to determine modal properties, which is essential for areas such as dispersion engineering within, e.g., supercontinuum generation or refractive index sensing with respect to bioanalytical applications.

APPENDIX A: FIRST-ORDER CORRECTION TERMS FOR THE FIELDS

In order to derive the first-order correction of the fields, let us consider Eq. (13). In this equation, we can write

$$\mathbb{F}_m^{(1)} = \frac{d\tilde{\mathbb{F}}}{d\Lambda}\Big|_{\Lambda=0} = \left\{ \frac{\partial\tilde{\mathbb{F}}}{\partial\Lambda} + \frac{\partial\tilde{\mathbb{F}}}{\partial\beta}\frac{\partial\beta}{\partial\Lambda} \right\}_{\Lambda=0}, \tag{A1}$$

where we define $\tilde{\mathbb{F}} = \mathbb{F}(\mathbf{r}_{||};\ \beta;\ \Lambda)$ with the tilde as the analytical continuation of β in the exterior of the fiber. Using the relations

$$\beta = \beta_m + \Lambda\beta_m^{(1)} + O(\Lambda^2) + \cdots \tag{A2}$$

and

$$\varkappa^2 + \beta^2 = (\varepsilon + \Lambda\Delta\varepsilon)(\mu + \Lambda\Delta\mu)(k_0 + \Lambda\Delta k_0)^2, \tag{A3}$$

we get

$$\frac{\partial\varkappa}{\partial\Lambda}\Big|_{\Lambda=0} = \frac{\Delta\varepsilon\mu k_0^2 + \varepsilon\Delta\mu k_0^2 + 2\varepsilon\mu k_0\Delta k_0}{2\varkappa_m} = \frac{\gamma}{2\varkappa_m}, \tag{A4}$$

$$\frac{\partial\varkappa}{\partial\beta}\Big|_{\Lambda=0} = \frac{-\beta_m}{\varkappa_m}. \tag{A5}$$

We know from solving Maxwell's equations in homogeneous and isotropic media that the z component of outgoing fields in the exterior have the form [1,31]

$$E_z = \sum_n E_{0n} H_n^{(1)}(\varkappa\rho) e^{in\phi}, \tag{A6}$$

$$H_z = \sum_n H_{0n} H_n^{(1)}(\varkappa\rho) e^{in\phi}, \tag{A7}$$

where $H_n^{(1)}(x)$ denotes Hankel functions of the first kind. The coefficients E_{0n} and H_{0n} correspond to transverse magnetic and transverse electric fields, respectively, while the full fields are a superposition of the two contributions. Hence, by applying Eq. (27) on the z component of the electric field, we have

$$\begin{aligned} E_{mz}^{(1)} &= \left(\frac{\partial\varkappa}{\partial\Lambda} + \beta_m^{(1)}\frac{\partial\varkappa}{\partial\beta}\right)\frac{\partial E_{mz}}{\partial\varkappa}\Big|_{\varkappa=\varkappa_m} \\ &= \left(\frac{\gamma}{2} - \beta_m\beta_m^{(1)}\right)\frac{\rho}{\varkappa_m^2}\frac{\partial E_{mz}}{\partial\rho}, \end{aligned} \tag{A8}$$

where we have applied Eqs. (30) as well as (31) and converted the $\varkappa$ derivative to a ρ derivative using the fact that Eq. (32) solely contains products of $\varkappa$ and ρ. The same steps can be carried out for the first-order correction of the magnetic field, resulting in a functional behavior identical to Eq. (34), except that the z components of the electric field are replaced by that of the magnetic field.

Next, we express $E_{m\phi}^{(1)}$ in dependence of the z components [32]:

$$E_\phi = \frac{i\beta}{\varkappa^2\rho}\frac{\partial E_z}{\partial\phi} - \frac{i(k_0+\Lambda\Delta k_0)(\mu+\Lambda\Delta\mu)}{\varkappa^2}\frac{\partial H_z}{\partial\rho}. \quad \text{(A9)}$$

By applying Eq. (27) to the above equation, we obtain the first-order correction term for the ϕ component of the electric field as

$$\begin{aligned} E_{m\phi}^{(1)} =& \left(\frac{i\varkappa_m^2\beta_m^{(1)} + 2i\beta_m^2\beta_m^{(1)} - i\beta_m\gamma}{\varkappa_m^4\rho}\right)\frac{\partial E_{mz}}{\partial\phi} \\ &+ \left(\frac{i\beta_m\gamma - 2i\beta_m^2\beta_m^{(1)}}{2\varkappa_m^4}\right)\frac{\partial^2 E_{mz}}{\partial\phi\partial\rho} \\ &+ \left(\frac{ik_0\mu\gamma - 2ik_0\mu\beta_m\beta_m^{(1)}}{2\varkappa_m^4} - \frac{i\Delta k_0\mu + i\Delta\mu k_0}{\varkappa_m^2}\right)\frac{\partial H_{mz}}{\partial\rho} \\ &+ \left(\frac{2ik_0\mu\rho\beta_m\beta_m^{(1)} - ik_0\mu\rho\gamma}{2\varkappa_m^4}\right)\frac{\partial^2 H_{mz}}{\partial\rho^2}. \end{aligned} \quad \text{(A10)}$$

For $H_{m\phi}^{(1)}$, we use the relation

$$H_\phi = \frac{i\beta}{\varkappa^2\rho}\frac{\partial H_z}{\partial\phi} + \frac{i(k_0+\Lambda\Delta k_0)(\varepsilon+\Lambda\Delta\varepsilon)}{\varkappa^2}\frac{\partial E_z}{\partial\rho}, \quad \text{(A11)}$$

which yields

$$\begin{aligned} H_{m\phi}^{(1)} =& \left(\frac{i\varkappa_m^2\beta_m^{(1)} + 2i\beta_m^2\beta_m^{(1)} - i\beta_m\gamma}{\varkappa_m^4\rho}\right)\frac{\partial H_{mz}}{\partial\phi} \\ &+ \left(\frac{i\beta_m\gamma - 2i\beta_m^2\beta_m^{(1)}}{2\varkappa_m^4}\right)\frac{\partial^2 H_{mz}}{\partial\phi\partial\rho} \\ &+ \left(\frac{2ik_0\varepsilon\beta_m\beta_m^{(1)} - ik_0\varepsilon\gamma}{2\varkappa_m^4} + \frac{i\Delta k_0\varepsilon + i\Delta\varepsilon k_0}{\varkappa_m^2}\right)\frac{\partial E_{mz}}{\partial\rho} \\ &+ \left(\frac{ik_0\varepsilon\gamma\rho - 2ik_0\varepsilon\rho\beta_m\beta_m^{(1)}}{2\varkappa_m^4}\right)\frac{\partial^2 E_{mz}}{\partial\rho^2}. \end{aligned} \quad \text{(A12)}$$

Substituting the above correction terms to Eq. (15) of the main text and using the relations in Eqs. (35) and (37) at $\Lambda = 0$ for the remaining ϕ components in the first line of Eq. (15), we obtain Eq. (16).

Funding. Deutsche Forschungsgemeinschaft (SPP 1839, WE 5815/5-1).

Disclosures. The authors declare no conflicts of interest.

REFERENCES

1. A. W. Snyder and J. Love, *Optical Waveguide Theory* (Springer, 2012).
2. P. Russell, "Photonic crystal fibers," Science **299**, 358–362 (2003).
3. R. Jha, J. Villatoro, and G. Badenes, "Ultrastable in reflection photonic crystal fiber modal interferometer for accurate refractive index sensing," Appl. Phys. Lett. **93**, 191106 (2008).
4. D. Monzón-Hernández and J. Villatoro, "High-resolution refractive index sensing by means of a multiple-peak surface plasmon resonance optical fiber sensor," Sens. Actuators B Chem. **115**, 227–231 (2006).
5. A. M. Pinto and M. Lopez-Amo, "Photonic crystal fibers for sensing applications," J. Sens. **2012**, 598178 (2012).
6. M. Calcerrada, C. Garca-Ruiz, and M. González-Herráez, "Chemical and biochemical sensing applications of microstructured optical fiber-based systems," Laser Photon. Rev. **9**, 604–627 (2015).
7. A. M. Zheltikov, "Let there be white light: supercontinuum generation by ultrashort laser pulses," Phys. Usp. **49**, 605 (2006).
8. I. Allayarov, M. Schmidt, and T. Weiss, "Theory of four-wave mixing for bound and leaky modes," Phys. Rev. A **101**, 043806 (2020).
9. T. Weiss, M. Mesch, M. Schäferling, H. Giessen, W. Langbein, and E. A. Muljarov, "From dark to bright: first-order perturbation theory with analytical mode normalization for plasmonic nanoantenna arrays applied to refractive index sensing," Phys. Rev. Lett. **116**, 237401 (2016).
10. I. Teraoka, S. Arnold, and F. Vollmer, "Perturbation approach to resonance shifts of whispering-gallery modes in a dielectric microsphere as a probe of a surrounding medium," J. Opt. Soc. Am. B **20**, 1937–1946 (2003).
11. A. Unger and M. Kreiter, "Analyzing the performance of plasmonic resonators for dielectric sensing," J. Phys. Chem. C **113**, 12243–12251 (2009).
12. W. Zhang and O. J. Martin, "A universal law for plasmon resonance shift in biosensing," ACS Photon. **2**, 144–150 (2015).
13. C. Sauvan, J.-P. Hugonin, I. Maksymov, and P. Lalanne, "Theory of the spontaneous optical emission of nanosize photonic and plasmon resonators," Phys. Rev. Lett. **110**, 237401 (2013).
14. Q. Bai, M. Perrin, C. Sauvan, J.-P. Hugonin, and P. Lalanne, "Efficient and intuitive method for the analysis of light scattering by a resonant nanostructure," Opt. Express **21**, 27371–27382 (2013).
15. E. A. Muljarov, W. Langbein, and R. Zimmermann, "Brillouin–Wigner perturbation theory in open electromagnetic systems," Europhys. Lett. **92**, 50010 (2011).
16. E. Muljarov and T. Weiss, "Resonant-state expansion for open optical systems: generalization to magnetic, chiral, and bi-anisotropic materials," Opt. Lett. **43**, 1978–1981 (2018).
17. J. Yang, H. Giessen, and P. Lalanne, "Simple analytical expression for the peak-frequency shifts of plasmonic resonances for sensing," Nano Lett. **15**, 3439–3444 (2015).
18. T. Weiss, M. Schäferling, H. Giessen, N. Gippius, S. Tikhodeev, W. Langbein, and E. Muljarov, "Analytical normalization of resonant states in photonic crystal slabs and periodic arrays of nanoantennas at oblique incidence," Phys. Rev. B **96**, 045129 (2017).
19. M. Mesch, T. Weiss, M. Schäferling, M. Hentschel, R. S. Hegde, and H. Giessen, "Highly sensitive refractive index sensors with plasmonic nanoantennas—utilization of optimal spectral detuning of Fano resonances," ACS Sens. **3**, 960–966 (2018).
20. S. Upendar, I. Allayarov, M. Schmidt, and T. Weiss, "Analytical mode normalization and resonant state expansion for bound and leaky modes in optical fibers-an efficient tool to model transverse disorder," Opt. Express **26**, 22536–22546 (2018).
21. I. Allayarov, S. Upendar, M. Schmidt, and T. Weiss, "Analytic mode normalization for the Kerr nonlinearity parameter: prediction of nonlinear gain for leaky modes," Phys. Rev. Lett. **121**, 213905 (2018).
22. S. Both and T. Weiss, "First-order perturbation theory for changes in the surrounding of open optical resonators," Opt. Lett. **44**, 5917–5920 (2019).
23. A. K. Ghatak and S. Lokanathan, *Quantum Mechanics: Theory and Applications* (Macmillan, 2004).
24. J. H. Lowry, J. S. Mendlowitz, and N. M. Subramanian, "Optical characteristics of teflon AF fluoroplastic materials," Opt. Eng. **31**, 1982–1986 (1992).
25. B. Keller, M. DeGrandpre, and C. Palmer, "Waveguiding properties of fiber-optic capillaries for chemical sensing applications," Sens. Actuators B Chem. **125**, 360–371 (2007).
26. F. Eftekhari, J. Irizar, L. Hulbert, and A. S. Helmy, "A comparative study of Raman enhancement in capillaries," J. Appl. Phys. **109**, 113104 (2011).
27. Y. Kayama, T. Ichikawa, and H. Ohno, "Transparent and colourless room temperature ionic liquids having high refractive index over 1.60," Chem. Commun. **50**, 14790–14792 (2014).
28. C. Jain, A. Braun, J. Gargiulo, B. Jang, G. Li, H. Lehmann, S. A. Maier, and M. A. Schmidt, "Hollow core light cage: trapping light behind bars," ACS Photon. **6**, 649–658 (2018).

29. B. Jang, J. Gargiulo, R. F. Ando, A. Lauri, S. A. Maier, and M. A. Schmidt, “Light guidance in photonic band gap guiding dual-ring light cages implemented by direct laser writing,” Opt. Lett. **44**, 4016–4019 (2019).
30. A. N. Bashkatov and E. A. Genina, “Water refractive index in dependence on temperature and wavelength: a simple approximation,” Proc. SPIE **5068**, 393–395 (2003).
31. T. White, B. Kuhlmey, R. McPhedran, D. Maystre, G. Renversez, C. M. De Sterke, and L. Botten, *Multipole Method for Microstructured Optical Fibers* (2002).
32. J. D. Jackson, *Classical Electrodynamics* (Wiley, 2007).